

measurements, varying again  $i$ ,  $j$ , and  $k$ . The results will be published in forthcoming papers. Together with the features of the macroscopic phase behavior summarized in the preceding sections, these data may then serve as basis for a consistent theory of the microstructure of these ternary systems.

*Note Added in Proof.* Since this paper was submitted, we have shown that the phase behavior of quinary systems of the type  $H_2O$ -oil-nonionic amphiphile-ionic amphiphile-salt evolves from a tricritical line that spans across five-dimensional space at 1 bar.<sup>11</sup>

*Acknowledgment.* We are indebted to Mrs. H. Frahm, Mr. B. Faulhaber, and Mr. T. Lieu for their assistance with the experiments, to Mr. D. Luckmann for drawing the figures, and to the Max-Buchner-Stiftung and the German Federal Ministry for Research and Technology (BMFT) for financial support.

(11) Kahlweit, M.; Strey, R., paper presented at the workshop "Progress in Microemulsions" at Erice, Oct 1985; to be submitted for publication in *J. Phys. Chem.*

## CHEMICAL KINETICS

### Mass Spectrometric Investigation and Computer Modeling of the $CH_4-O_2-O_3$ Reaction from 480 to 830 K

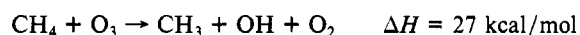
G. Rotzoll

*Institut für Technische Chemie, Universität Hannover, 3000 Hannover 1, Federal Republic of Germany*  
(Received: February 20, 1985; In Final Form: June 30, 1985)

The reaction of methane with ozonized oxygen was investigated in a molecular beam source reactor, consisting of a heated 1-mm-diameter alumina flow tube equipped with a 0.2-mm nozzle. Typical values for pressure and residence time were 600 mbar and 16 ms, respectively, and the temperature range covered was from 480 to 830 K. The gas mixture expanding from the reactor was transformed into a molecular beam and analyzed by a mass spectrometer.  $H_2O$ ,  $CO$ ,  $CH_2O$ ,  $CH_3OH$ ,  $H_2O_2$ ,  $CO_2$ , and  $CH_3OOH$  were found as reaction products. The experimental results could be fairly well modeled by a reaction mechanism consisting of 47 elementary reactions with 21 species. A kinetic sensitivity analysis and investigation of the reaction pathways yields the main mechanistic features of the reaction. The reaction is initiated by the thermal decomposition of ozone. Very important in the reaction are secondary reactions of ozone with methyl radicals and hydrogen atoms. Besides that, radical-radical reactions of methyl and methylperoxy radicals play a dominant role in the course of the reaction.

#### Introduction

Ozone can initiate oxidation reactions of alkanes at temperatures where, in the absence of ozone, reaction progress would only be very slow.<sup>1-5</sup> The simplest alkane reaction, the reaction of methane with ozonized oxygen, was studied by Schubert and Pease,<sup>6</sup> Dillemath et al.,<sup>7</sup> and Kleimenov and Nalbandian.<sup>8</sup> The experiments of the first two groups were carried out in static systems at low temperatures and rather long reaction times. Products observed by infrared absorption analysis were  $CO$ ,  $CO_2$ ,  $HCOOH$ , and  $H_2O$ . The disappearance of ozone was analyzed in terms of a second-order reaction with methane, resulting in an activation energy of about 15 kcal/mol. The only conceivable elementary reaction between  $CH_4$  and  $O_3$ , however, as pointed out by Atkinson and Carter,<sup>9</sup> is



The activation energy of this hypothetical reaction can be expected to lie even above 27 kcal/mol, thus being higher than the activation energy for the thermal decomposition of ozone, which equals 23 kcal/mol.<sup>10</sup> A direct reaction between  $CH_4$  and  $O_3$  is therefore severely in doubt.

More in line with the thermodynamic facts, the results of Kleimenov and Nalbandian,<sup>8</sup> obtained in a flow system at 423 K and residence times of 6 to 32 s, were interpreted in terms of the thermal decomposition of ozone with subsequent reaction of O atoms with  $CH_4$ . This conclusion was arrived at by noting that the ozone decomposition temperature coincided with the temperature at which the oxidation of methane proceeded at a measurable rate. These authors also reported methyl hydroperoxide and formaldehyde as the principal reaction products, completely different from the results obtained by Schubert and Pease and Dillemath et al. None of the studies mentioned has resulted in an analysis of the overall reaction in terms of elementary reactions.

The objective of the work presented in this article therefore is to provide a better and, above all, more quantitative understanding of the ozone-initiated methane oxidation. The experimental ar-

(1) Dardin, V. J.; Albright, L. F. *Ind. Eng. Chem. Proc. Des. Develop.* **1965**, *4*, 61.

(2) Caprio, V.; Insola, A.; Barbella, R. *Combust. Inst. Europ. Symp.* **1973**, *99*.

(3) Caprio, V.; Insola, A.; Lignola, P. G. *Combust. Inst. Europ. Symp.* **1975**, *85*.

(4) Caprio, V.; Insola, A.; Lignola, P. G. *Combust. Sci. Technol.* **1979**, *20*, 19.

(5) Caprio, V.; Insola, A.; Lignola, P. G. *Combust. Sci. Technol.* **1984**, *35*, 215.

(6) Schubert, C. C.; Pease, R. N. *J. Am. Chem. Soc.* **1956**, *78*, 2044.

(7) Dillemath, F. J.; Skidmore, D. R.; Schubert, C. C. *J. Phys. Chem.* **1960**, *64*, 1496.

(8) Kleimenov, N. A.; Nalbandian, A. B. *Proc. Acad. Sci. USSR, Phys. Chem.* **1958**, *122*, 667.

(9) Atkinson, R.; Carter, W. P. L. *Chem. Rev.* **1984**, *84*, 437.

(10) Baulch, D. L.; Drysdale, D. D.; Duxbury, J.; Grant, S. "Evaluated Kinetic Data for High Temperature Reactions"; Butterworths: London, 1976; Vol. 3.

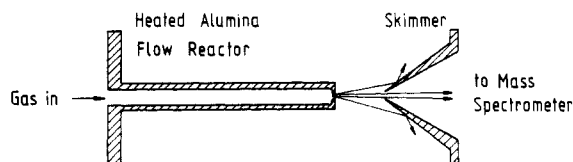


**Figure 1.** Principle of the molecular beam source reactor with a nozzle.

rangement uses molecular beam sampling with mass spectrometric detection thus facilitating complete product analysis. The experimental data obtained are compared with values computed via a kinetic model containing mainly published rate constants with only a few modifications.

### Experimental Section

The experimental method employed is a variant of the molecular beam source reactor (MBSR) that has been fully described before.<sup>11</sup> The basic principle of the method is shown in Figure 1. A gas mixture enters the alumina reactor at room temperature and is rapidly heated by conduction from the tube wall. Depending on the temperature level of the reactor, reaction takes place in the gas as it flows toward the reactor exit. At the exit, the reacting gas mixture expands through a small nozzle by which chemical reactions are frozen on a time scale of a few microseconds and a molecular beam is formed that is skimmed, collimated, and analyzed by a mass spectrometer. By changing the reactor temperature, the principal experimental variable, the various stages of the reaction, beginning with the initiation and ending with final products, can be investigated.

The modification of the present reactor compared to the ones used in ref 11 concerns the nozzle at the reactor exit. If a tube with a straight through bore is used, a considerable nonlinear pressure drop develops along the axial direction. With a nozzle, the pressure drop is transferred almost completely into the nozzle with Poiseuille-type flow at nearly constant pressure in the main part of the tube. This different pressure characteristic affects the residence time of the reactor that is larger than for a tube without nozzle. Apart from this modification, all other details including the assembly of the tube, heating of the reactor, apparatus, etc. are as described in ref 11. The pressure at the reactor entrance was measured with a mechanical pressure gauge. The actual MBSR used in this work had a length of 15 cm, an internal bore of 0.11 cm, and a nozzle diameter of 0.02 cm.

As described in ref 11, the ceramic tube is glued into a brass flange to enable its mounting as the beam source. Therefore, this end of the reactor has to be water-cooled to prevent decomposition of the adhesive. The axial temperature of the reactor thus is nonuniform and consists of a region of increasing temperature followed by a region of nearly constant temperature. The axial temperature profiles, needed for the calculations described in the next section, were obtained by the methods described in ref 11. The shapes of the profiles were obtained by solving the differential equations of the tube heat balance as a function of heating power and the exit temperatures were obtained by measuring flight times of an argon beam.

The Reynolds numbers employed in the present work are always <300, so that the gas flow is laminar giving rise to radially nonuniform flow velocities and radial concentration and temperature gradients. These effects are counteracted by radial diffusion and thermal conduction, most effective for small tube diameters. A full computational treatment of these effects for a large reaction mechanism would be prohibitive and therefore the one-dimensional approximation is adopted. In view of these simplifying assumptions, axial thermal conduction and diffusion is also neglected.

The question on the occurrence of wall reactions because of the large surface-to-volume ratios of the MBSR's has been considered before.<sup>11</sup> It was shown among other things that the thermal decomposition of ozone could be modeled by a purely homogeneous kinetic model without interference from wall reactions. The

experiment on the thermal decomposition of ozone was repeated with the reactor used in this work and the data were compared with calculations based on the same homogeneous kinetic model. As in ref 11, good agreement was obtained between experimental data and calculated values. The present reaction system, however, is much more complicated and many more radical species are present. It is difficult to come to a general conclusion as to the importance of wall reactions for all these species, but some conclusions can be drawn from kinetic calculations by including wall reactions explicitly. These results will be discussed later.

Methane (99.5%) and oxygen (99.998%) were used directly from cylinders without further purification. The oxygen flow was passed through a commercial ozone generator that could produce up to 5% ozone. The flow rates of methane and ozonized oxygen were adjusted by two thermal mass flow controllers. The two gas streams were mixed just outside the molecular beam sampling apparatus and flowed through a stainless steel tube into the MBSR. As reaction products could only be detected with reactor temperatures above ca. 500 K, it is concluded that no reaction occurred between the mixing point and the MBSR. This conclusion is confirmed by calculations with the reaction mechanism described later, which gives negligible extent of reaction in the gas during the flow from the mixing point to the reactor.

The composition of the gas leaving the reactor was measured by taking the mass spectra of the molecular beams formed. In order to avoid extensive fragmentation in the mass spectra and still have sufficient sensitivity, a value of 20 eV was chosen for the ionization energy. Spectra were taken for reactor temperatures from room temperature to 830 K. Reaction products became detectable above about 500 K. The following products were identified: H<sub>2</sub>O (*m/e* 18), CO (*m/e* 28 after subtraction of contribution from CH<sub>2</sub>O), CH<sub>2</sub>O (*m/e* 29, 30), CH<sub>3</sub>OH (*m/e* 31), H<sub>2</sub>O<sub>2</sub> (*m/e* 34 after subtraction of contribution from O<sub>2</sub>), CO<sub>2</sub> (*m/e* 44), and CH<sub>3</sub>OOH (*m/e* 47, 48). Weak signals increasing with reactor temperature were also found on masses 45 and 46 and are attributed to HCOOH. Ethane could not be detected in significant amounts. There is interference from CO and CH<sub>2</sub>O on masses 28 to 30, but also no signals above the noise level were recorded on masses 26 and 27 that are present in the mass spectrum of ethane at 20 eV too. The signal on mass 47 may come from both methyl hydroperoxide<sup>12</sup> and from the methylperoxy radical.<sup>13</sup> Since the temperature dependence of the signal on mass 48 (due to both O<sub>3</sub> and CH<sub>3</sub>OOH) displays a shoulder at the maximum of the signal on mass 47, the latter at least partly may be attributed to CH<sub>3</sub>OOH. A contribution from the peroxy radical, however, cannot be ruled out and is also supported by the kinetic calculations. It should finally be noted that there was no detectable reaction with the ozone generator turned off. The initiation of the reaction under the given conditions of residence times and temperatures is therefore solely due to the presence of ozone.

In order to convert the measured ion signals into mole fractions, calibrations were performed where possible. The concentration of ozone in oxygen was measured by absorption at 253.7 nm with an UV photometer. Calibration mixtures for H<sub>2</sub>O and CH<sub>3</sub>OH were prepared by passing O<sub>2</sub> through a thermostated saturator containing the respective liquid. The calibrations were performed under identical conditions of CH<sub>4</sub> and O<sub>2</sub> concentrations, temperatures, and flow rates as in the actual experiments, but without ozone. CO and CO<sub>2</sub> were calibrated against O<sub>2</sub> by preparing mixtures with the mass flow controllers. The calibration factor for CH<sub>2</sub>O was obtained in the following way: a CH<sub>2</sub>O/O<sub>2</sub> beam was produced by heating paraformaldehyde powder to about 95 °C in a stainless steel container mounted just before the reactor tube with O<sub>2</sub> flowing over it. No reaction occurred under these conditions and no polymers of CH<sub>2</sub>O were detected in the beam. The pressure of CH<sub>2</sub>O relative to O<sub>2</sub> was obtained by dividing the ratio of the sum of the ion signals due to CH<sub>2</sub>O and O<sub>2</sub>,

(12) DeCorpo, J. J.; McDowell, M. V.; Sheinson, R. S.; Wyatt, J. R. *J. Chem. Soc., Chem. Commun.* **1974**, 86, 533.

(13) Washida, N.; Bayes, K. D. *Int. J. Chem. Kinet.* **1976**, 8, 777.

(11) Rotzoll, G. *Int. J. Chem. Kinet.* **1984**, 16, 1401.

TABLE I: Experimental Conditions

mass flow rate, g/s	$x_{\text{CH}_4}$	$x_{\text{O}_2}$	$x_{\text{O}_3}$	$p,^a$ mbar	$T, \text{K}$	$\tau, \text{ms}$
$2.15 \times 10^{-3}$	0.666	0.319	0.015	360-470	480-830	14.8-15.5
$3.22 \times 10^{-3}$	0.500	0.479	0.021 <sup>b</sup>	500-650	480-830	15.6-16.5
$3.58 \times 10^{-3}$	0.334	0.636	0.030	500-680	480-830	15.7-16.7

<sup>a</sup> Initial pressures. Calculated pressure drops <3%. <sup>b</sup>  $x_{\text{O}_3}$  at this flow rate and mixture composition was varied between 0.007 and 0.021 with corresponding variation of  $x_{\text{O}_2}$ .

respectively, measured at 70-eV ionization energy, by the ratio of the ionization cross sections. The ionization cross section of CH<sub>2</sub>O was calculated from a semiempirical formula.<sup>14</sup> With the pressure ratio thus obtained, the calibration factor at 20 eV could be determined. Calibration factors for the unstable peroxides relative to O<sub>2</sub> were arbitrarily set equal to one because of lack of other suitable information.

The accuracy of the experimental mole fractions obtained in the way described depends on several factors such as signal-to-noise ratio of the measured intensities, reproducibility, and precision of calibration. It is estimated that the accuracy of most mole fractions should be about 10%. For CO and CO<sub>2</sub> the background is rather large, so that for these compounds the errors may be considerably larger.

## Results

The experimental conditions for which experiments were performed are summarized in Table I. In all experiments the reactor temperature was varied at constant mass flow rate, so that the pressures varied accordingly. The calculated residence times, on the other hand, vary only slightly. It should be recalled that the reactor temperature is not uniform along the reactor but increases in the first part followed by a region of nearly constant temperature. This temperature profile is fully accounted for in the calculations.

A comparison of the results obtained for the different conditions of Table I yielded no marked differences apart from shifts in the magnitude of the product mole fractions. Decreasing the initial

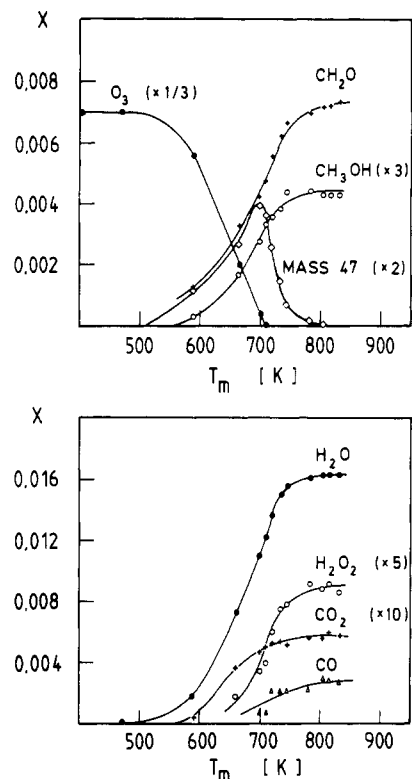


Figure 2. Measured mole fractions vs. maximal gas temperatures. Experimental conditions given in the second row of Table I.  $x_{\text{O}_3} = 0.021$ .

ozone concentration at nearly constant methane to oxygen ratio had the effect of decreasing all product concentrations. Therefore, detailed results are presented here only for the mixture composition given in the second row of Table I. The reaction mechanism presented below, however, has been designed to fit all available experimental data simultaneously.

Figure 2 shows the measured mole fractions as a function of the maximal gas temperature. The experimental conditions are given in the second row of Table I. Mole fractions of CH<sub>4</sub> and O<sub>2</sub> are not shown as these change only slightly because of the small overall conversions. The temperatures in Figure 2 have been determined by taking the heat release due to the chemical reaction into account. The procedure by which this is done will be explained when the modeling calculations are discussed. It is seen that the products begin to appear simultaneously with the decrease of ozone. The concentrations of all products, with the exception of methylperoxy/methyl hydroperoxide, increase with temperature and tend to level off around 800 K after the disappearance of ozone and methyl hydroperoxide and/or the methylperoxy radical.

To provide a detailed understanding of the reaction progress with temperature, we performed calculations with a kinetic mechanism assembled mainly from literature data. The calculations involve the solution of the coupled fluid dynamic and chemical equations as described in ref 11. Two modifications in the computations, however, were introduced for the present reactor and reaction. First, since the residence time in the nozzle is negligible compared to the residence time in the reactor, integration of the differential equations need only be performed up to the nozzle. This means a considerable simplification, since a normal initial value problem has to be solved and no iteration is needed to obtain the boundary conditions that the final Mach number must be equal to unity.

The second modification concerns the heat release of the chemical reaction that turned out to have an influence on the reactor temperature profile in this rather low-temperature range. Mathematically, this means an additional term in the second-order differential equation for the axial reactor temperature profile. In the computational procedure, the mutual influence of chemical reaction and reactor temperature was solved by iteration. Starting from the reactor temperature profile, without taking the heat release of chemical reaction into account, we solved the fluid

- (14) Beran, J. A.; Kevan, L. J. *J. Chem. Phys.* **1969**, *73*, 3866.  
 (15) Ogryzolo, E. A.; Paltenghi, R.; Bayes, K. D. *Int. J. Chem. Kinet.* **1981**, *13*, 667.  
 (16) Baulch, D. L.; Cox, R. A.; Crutzen, P. J.; Hampson, Jr. R. F.; Kerr, J. A.; Troe, J.; Watson, R. T. *J. Phys. Chem. Ref. Data* **1982**, *11*, 327.  
 (17) Warnatz, J.; Bockhorn, H.; Möser, A.; Wenz, H. W. *Symp. (Int.) Combust. [Proc.]*, **19th** **1982**, 197.  
 (18) Warnatz, J. *Combust. Sci. Technol.* **1981**, *26*, 203.  
 (19) Walker, R. W. In "Gas Kinetics and Energy Transfer"; Ashmore, P. G.; Donovan, R. J., Eds.; Chemical Society: London, 1977; Vol. 2, p 269.  
 (20) Borrell, P.; Cobos, C. J.; Croce de Cobos, A. E.; Hippler, H.; Luther, K.; Ravishankara, A. R.; Troe, J. *Ber. Bunsenges. Phys. Chem.* **1985**, *89*, 337.  
 (21) Parkes, D. A. *Int. J. Chem. Kinet.* **1977**, *9*, 451.  
 (22) Benson, S. W. *Prog. Energy Combust. Sci.* **1981**, *7*, 125.  
 (23) Niki, H.; Maker, P. D.; Savage, C. M.; Breitenbach, L. P. *J. Phys. Chem.* **1983**, *87*, 2190.  
 (24) Baulch, D. L.; Duxbury, J. *Combust. Flame* **1980**, *37*, 313.  
 (25) Gutman, D.; Sanders, N.; Butter, J. E. *J. Phys. Chem.* **1982**, *86*, 66.  
 (26) Demerjian, K. L.; Kerr, J. A.; Calvert, J. G. *Adv. Environ. Sci. Technol.* **1974**, *4*, 1.  
 (27) Quee, M. J. Y.; Thynne, J. C. *J. Trans. Faraday Soc.* **1966**, *62*, 3154.  
 (28) Colket III, M. B.; Naegeli, D. W.; Glassman, I. *Symp. (Int.) Combust., [Proc.]*, **16th** **1977**, 841.  
 (29) Hsu, D. S. Y.; Shaub, W. M.; Creamer, T.; Gutman, D.; Lin, M. C. *Ber. Bunsenges. Phys. Chem.* **1983**, *87*, 909.  
 (30) Lloyd, A. C. *Int. J. Chem. Kinet.* **1974**, *6*, 169.  
 (31) Engleman, V. S. "Survey and Evaluation of Kinetic Data on Reactions in Methane/Air Combustion", Report No. EPA-600/2-76-003, 1976.  
 (32) Dove, J. E.; Warnatz, J. *Ber. Bunsenges. Phys. Chem.* **1983**, *87*, 1040.  
 (33) Meier, U.; Grotheer, H. H.; Riekert, G.; Just, Th. *Ber. Bunsenges. Phys. Chem.* **1985**, *89*, 325.  
 (34) Grotheer, H. H.; Riekert, G.; Meier, U.; Just, Th. *Ber. Bunsenges. Phys. Chem.* **1985**, *89*, 187.  
 (35) Adams, G. F. Technical Report ARBRL-TR-02143, Aberdeen Proving Ground, MD, 1979.  
 (36) Laidler, K. J. "Theories of Chemical Reaction Rates"; McGraw-Hill: New York, 1969; p 118.  
 (37) Simonaitis, R.; Heicklen, J. *J. Phys. Chem.* **1975**, *79*, 298.

TABLE II: Reaction Mechanism for Ozone-Initiated Methane Oxidation from 480 to 830 K<sup>a</sup>

	reaction	log <i>A</i>	<i>E</i>	<i>n</i>	ref
(1)	O <sub>3</sub> + M → O + O <sub>2</sub> + M	14.64	22.71	0.00	10
(2)	O <sub>3</sub> + O → O <sub>2</sub> + O <sub>2</sub>	12.72	4.15	0.00	10
(3)	O <sub>3</sub> + CH <sub>3</sub> → O <sub>2</sub> + CH <sub>2</sub> O + H	10.30	0.00	0.71	15 <sup>b</sup>
(4)	O <sub>3</sub> + H → O <sub>2</sub> + OH	13.93	0.95	0.00	16
(5)	O + HO <sub>2</sub> → O <sub>2</sub> + OH	13.30	0.00	0.00	16
(6)	O + H <sub>2</sub> O <sub>2</sub> → OH + HO <sub>2</sub>	12.80	4.96	0.00	16
(7)	OH + HO <sub>2</sub> → H <sub>2</sub> O + O <sub>2</sub>	13.70	0.00	0.00	16
(8)	OH + H <sub>2</sub> O <sub>2</sub> → H <sub>2</sub> O + HO <sub>2</sub>	12.20	0.32	0.00	16
(9)	H + O <sub>2</sub> + M → HO <sub>2</sub> + M	18.81	0.00	-1.00	16
(10)	H + HO <sub>2</sub> → O <sub>2</sub> + H <sub>2</sub>	13.40	0.69	0.00	17
(11)	H + HO <sub>2</sub> → OH + OH	14.18	1.00	0.00	17
(12)	HO <sub>2</sub> + HO <sub>2</sub> → H <sub>2</sub> O <sub>2</sub> + O <sub>2</sub>	10.40	-2.38	0.00	16
(13)	H <sub>2</sub> O <sub>2</sub> + M → OH + OH + M	17.48	45.41	0.00	18
(14)	CH <sub>4</sub> + O → CH <sub>3</sub> + OH	7.08	7.62	2.10	17
(15)	CH <sub>4</sub> + OH → CH <sub>3</sub> + H <sub>2</sub> O	6.10	2.46	2.10	17 <sup>b</sup>
(16)	CH <sub>4</sub> + H → CH <sub>3</sub> + H <sub>2</sub>	4.34	8.75	3.00	17
(17)	CH <sub>4</sub> + HO <sub>2</sub> → CH <sub>3</sub> + H <sub>2</sub> O <sub>2</sub>	11.30	14.94	0.00	19
(18)	CH <sub>3</sub> + O <sub>2</sub> → CH <sub>3</sub> O <sub>2</sub>	11.15	0.00	0.00	20
(19)	CH <sub>3</sub> O <sub>2</sub> → CH <sub>3</sub> + O <sub>2</sub>	12.94	25.65	0.00	20
(20)	CH <sub>3</sub> O <sub>2</sub> + CH <sub>3</sub> O <sub>2</sub> → CH <sub>3</sub> OH + CH <sub>2</sub> O + O <sub>2</sub>	11.10	0.00	0.00	16
(21)	CH <sub>3</sub> O <sub>2</sub> + CH <sub>3</sub> O <sub>2</sub> → CH <sub>3</sub> O + CH <sub>3</sub> O + O <sub>2</sub>	11.00	0.00	0.00	16
(22)	CH <sub>3</sub> O <sub>2</sub> + CH <sub>3</sub> → CH <sub>3</sub> O + CH <sub>3</sub> O	13.00	0.00	0.00	21, fit
(23)	CH <sub>3</sub> O <sub>2</sub> + O → CH <sub>2</sub> O + H + O <sub>2</sub>	13.30	0.00	0.00	13
(24)	CH <sub>3</sub> O <sub>2</sub> + HO <sub>2</sub> → CH <sub>3</sub> OOH + O <sub>2</sub>	10.70	-2.58	0.00	16
(25)	CH <sub>3</sub> OOH → CH <sub>3</sub> O + OH	15.40	43.00	0.00	22 <sup>c</sup>
(26)	CH <sub>3</sub> OOH + OH → H <sub>2</sub> O + CH <sub>3</sub> O <sub>2</sub>	12.75	0.00	0.00	23 <sup>d</sup>
(27)	CH <sub>3</sub> OOH + OH → H <sub>2</sub> O + CH <sub>2</sub> O + OH	12.64	0.00	0.00	23 <sup>d</sup>
(28)	CH <sub>3</sub> + CH <sub>3</sub> → C <sub>2</sub> H <sub>6</sub>	13.30	0.00	0.00	24
(29)	CH <sub>3</sub> O + O <sub>2</sub> → CH <sub>2</sub> O + HO <sub>2</sub>	10.75	2.68	0.00	25 <sup>b</sup>
(30)	CH <sub>3</sub> O + CH <sub>3</sub> O → CH <sub>3</sub> OH + CH <sub>2</sub> O	13.20	0.00	0.00	26
(31)	CH <sub>3</sub> O + HO <sub>2</sub> → CH <sub>3</sub> OH + O <sub>2</sub>	12.70	0.00	0.00	fit
(32)	CH <sub>3</sub> O + CH <sub>3</sub> → CH <sub>4</sub> + CH <sub>2</sub> O	13.00	0.00	0.00	27
(33)	CH <sub>3</sub> + HO <sub>2</sub> → CH <sub>3</sub> O + OH	12.90	0.00	0.00	28, fit
(34)	CH <sub>2</sub> O + O → CHO + OH	6.23	1.48	2.32	29
(35)	CH <sub>2</sub> O + O → CO <sub>2</sub> + H + H	5.60	1.36	2.42	29 <sup>b</sup>
(36)	CH <sub>2</sub> O + OH → CHO + H <sub>2</sub> O	4.74	-0.19	2.65	29 <sup>b</sup>
(37)	CH <sub>2</sub> O + H → CHO + H <sub>2</sub>	9.46	2.63	1.27	29
(38)	CH <sub>2</sub> O + HO <sub>2</sub> → CHO + H <sub>2</sub> O <sub>2</sub>	12.00	8.00	0.00	30
(39)	CH <sub>2</sub> O + CH <sub>3</sub> → CHO + CH <sub>4</sub>	10.00	6.00	0.50	31
(40)	CHO + O <sub>2</sub> → CO + HO <sub>2</sub>	12.48	0.00	0.00	16
(41)	CH <sub>3</sub> OH + O → CH <sub>3</sub> O + OH	12.40	4.71	0.00	32 <sup>e</sup>
(42)	CH <sub>3</sub> OH + OH → CH <sub>3</sub> O + H <sub>2</sub> O	12.22	1.58	0.00	33
(43)	CH <sub>3</sub> OH + H → CH <sub>3</sub> O + H <sub>2</sub>	13.00	6.09	0.00	32 <sup>e</sup>
(44)	CH <sub>3</sub> OH + O → CH <sub>2</sub> OH + OH	12.88	4.71	0.00	32 <sup>e</sup>
(45)	CH <sub>3</sub> OH + OH → CH <sub>2</sub> OH + H <sub>2</sub> O	12.70	1.58	0.00	33
(46)	CH <sub>3</sub> OH + H → CH <sub>2</sub> OH + H <sub>2</sub>	13.48	6.09	0.00	32 <sup>e</sup>
(47)	CH <sub>2</sub> OH + O <sub>2</sub> → HO <sub>2</sub> + CH <sub>2</sub> O	12.76	0.00	0.00	34

<sup>a</sup> Rate constants given as  $k = AT^n \exp[-E/RT]$ . Units of  $k$  s<sup>-1</sup>, cm<sup>3</sup>/(mol s), or cm<sup>6</sup>/(mol<sup>2</sup> s). Activation energies in kcal/mol. <sup>b</sup> Rate constants adjusted within experimental error limits. <sup>c</sup> *A* factor reduced by a factor of 1.6. See text. <sup>d</sup> *A* factors slightly increased by a factor of 1.7 roughly corresponding to an activation energy of 0.5 kcal/mol. <sup>e</sup> Branching ratio CH<sub>2</sub>OH/CH<sub>3</sub>O assumed to be the same as for CH<sub>3</sub>OH + OH.<sup>33</sup>

dynamic and chemical equations and the solution yielded among other things the heat production terms needed for the reactor temperature balance. The temperature profile was then recalculated with these terms and so on until mutual consistency was achieved.

It is clear that the maximal gas temperatures, for a chemical reaction with the described effect on the reactor temperature, are not equal to the temperatures obtained from the time-of-flight experiments with Ar as gas. However, by comparing calculated temperatures of Ar and the reacting gas mixture at the same electric heating power, the increase of temperature in the reacting gas relative to Ar can be given. This is the way in which the temperatures in Figure 2 have been obtained.

**Reaction Mechanism.** The reaction mechanism used to simulate the experimental data is given in Table II. This reaction scheme is the final result after considerable experimentation with variation of key rate constants and initially many more reactions. In order to keep the set of reactions at a reasonable size, reactions with only a minor influence were excluded. The criterion chosen for this was that reactions contributing less than 5% to the formation or destruction of any species on a cumulative basis were omitted from the mechanism. Thus the initial set of reactions was much larger and included all possible radical-stable molecule and rad-

ical-radical reactions. Rate constants were taken from the literature if available or given reasonable estimates otherwise.

Most of the rate constants in Table II are at their literature values. Only a few are modified within their error limits, and only three are fitted. The significance of various reactions will be discussed in the next section, but a number of comments seem appropriate here. (1) Initiation of the reaction can only be achieved by the thermal decomposition of ozone, reaction 1. Reactions with higher activation energies like the hypothetical direct reaction between CH<sub>4</sub> and O<sub>3</sub> would not describe the temperature dependence of the onset of reaction properly and can therefore be excluded. (2) In the reaction between ozone and methyl radicals, reaction 3, it is not known experimentally if O<sub>2</sub> + CH<sub>3</sub>O or O<sub>2</sub> + CH<sub>2</sub>O + H, or both are the reaction products. Adams<sup>35</sup> has performed a RRKM calculation for the thermal decomposition of CH<sub>3</sub>O. With his frequency data and the assumption of 50% of the exothermicity of reaction 3 released as internal energy of CH<sub>3</sub>O, an estimate of  $2 \times 10^{13}$  s<sup>-1</sup> is obtained for the decomposition rate constant of the chemically activated CH<sub>3</sub>O from the quantum RRK formula.<sup>36</sup> On the other hand, deactivation at 700 K and 700 mbar proceeds at about  $3 \times 10^9$  s<sup>-1</sup>. Because of this ratio, instantaneous decomposition of CH<sub>3</sub>O into CH<sub>2</sub>O + H has been assumed in reaction 3. (3) Reaction

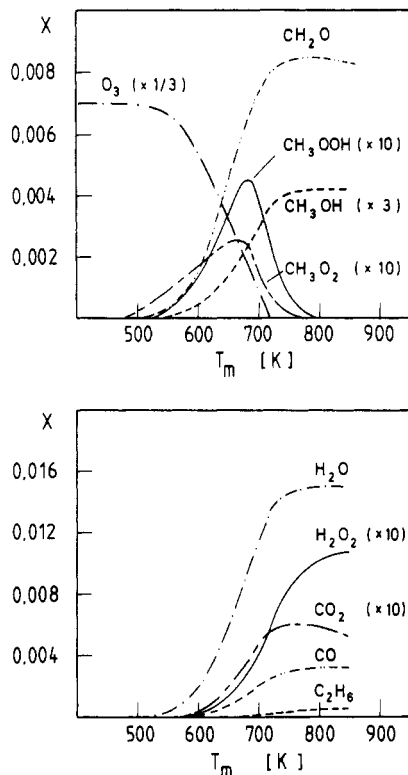


**Figure 3.** Calculated mole fractions vs. maximal gas temperatures. Same conditions as in Figure 2.

18 and 19 are in the falloff region under the present conditions. The value given for reaction 18 has been calculated according to the procedure given in ref 16 and the parameters given in ref 20 for the mean pressure and temperature of this work. The rate constant for reaction 19 is obtained from  $k_{18}$  and the equilibrium constant. Minor variations of  $k_{18}$  with corresponding variations of  $k_{19}$  have almost no effect, since an equilibrium is established between CH<sub>3</sub> and CH<sub>3</sub>O<sub>2</sub>. (4) The reactions of H and O with CH<sub>3</sub>OOH have not yet been measured. The rate constants of these reactions have been estimated to be the same as for H, O + CH<sub>3</sub>OH. With such values, however, these reactions turned out to be negligible under the criterion formulated above. For the second pathway of the reaction with OH, reaction 27, instantaneous decomposition of the intermediate CH<sub>2</sub>O<sub>2</sub>H into CH<sub>2</sub>O + OH has been assumed. (5) The branching ratio for CH<sub>2</sub>OH/CH<sub>3</sub>O production from CH<sub>3</sub>OH by attack of H, O, and OH has only been measured for OH at room temperature.<sup>33</sup> The same branching ratio is assumed here for the other reactions. This problem is only of minor importance for the present reaction, since only a small amount of the methanol formed is further attacked by the atoms and radicals as will be discussed below.

Figure 3 shows the reaction progress as a function of temperature, calculated with the mechanism of Table II for the experimental conditions given in the second row of Table I. As mentioned above, the mechanism was designed to fit all available experimental data from Table I. Reasonable agreement between the measured and calibrated product mole fractions and the calculated values could be achieved by modifying a number of rate constants within their experimental error limits and by fitting  $k_{22}$ ,  $k_{31}$ , and  $k_{33}$ . Analysis of the main reaction pathways and kinetic sensitivity analysis, discussed in the next section, were used to establish these modifications. It was not possible to model the mole fraction of methanol without introduction of reaction 31, for which no rate constant was found in the literature. This rate constant was therefore treated as a fitting parameter. For the other fitted rate constants,  $k_{22}$  and  $k_{33}$ , literature values do exist,<sup>21,28</sup> which were obtained indirectly, however. The present value of  $k_{22}$  is lower by a factor of 4 and that of  $k_{33}$  by a factor of 2.5. The reaction between methyl and hydroperoxy radicals is also quite important for high-temperature oxidation of methane and a direct determination of its rate constant is urgently needed.

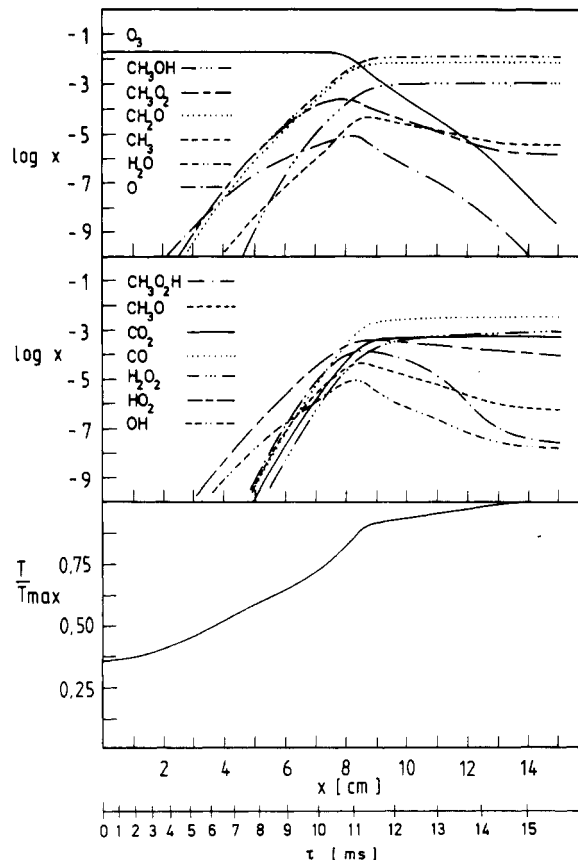


**Figure 4.** Calculated axial temperature and species profiles for a maximal gas temperature of 833 K and an initial pressure of 650 mbar. Other conditions are the same as in Figure 2.

The general agreement between measured and calculated mole fractions is good and within the estimated error limits of the experimental data. A somewhat larger discrepancy is found for CH<sub>2</sub>O, which may, however, be due to the indirect calibration method employed. For the uncalibrated products H<sub>2</sub>O<sub>2</sub> and CH<sub>3</sub>OOH/CH<sub>3</sub>O<sub>2</sub>, only qualitative agreement can be expected. The calculation shows that the mole fractions of CH<sub>3</sub>OOH and CH<sub>3</sub>O<sub>2</sub> are of comparable magnitude and that the signal on mass 47 may indeed be due to both species. The reason for the disappearance of methyl hydroperoxide above 700 K is its thermal instability and decomposition through reaction 25. The agreement of the experimental maximum with temperature could be somewhat improved by reducing the frequency factor given in ref 22 by a factor of 1.6. The reaction should be somewhat below the high-pressure limit under the present conditions. The formation of ethane, in correspondence with the experimental observations, turns out to be only of minor importance.

Figure 4 represents the details of a calculation for a maximal gas temperature of 833 K. Shown are the more important mole fractions and the gas temperature as a function of the reactor length. An additional time scale is included at the bottom. The reaction rapidly starts as the temperature rises and leads to a clearly visible additional temperature rise at an axial distance of about 9 cm. The main conversion has already occurred up to about 10 cm and only the concentrations of ozone, the radicals, and methyl hydroperoxide continue to decrease noticeably with the reactor length.

## Discussion

**Possible Influence of Wall Reactions.** The problem of possible interference from wall reactions was noted in the Experimental Section. This question can be partly answered by explicitly including wall reactions in the calculations and investigating the changes that are produced in the calculated mole fractions of the measured species. The type of wall reactions considered are the disappearance of atom and radical species at the wall by recombination or other reactions. These reactions are formulated as

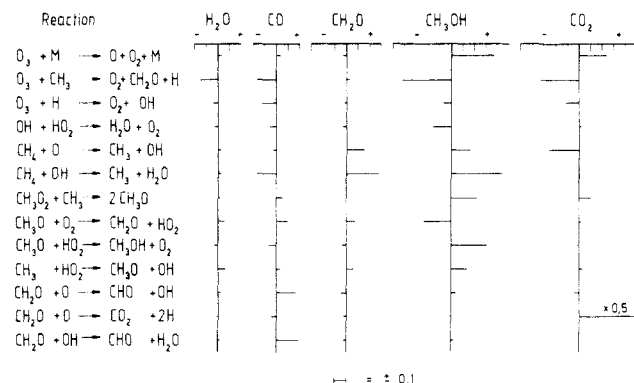


**Figure 5.** Integral sensitivity coefficients,  $\Delta \ln x_i / \Delta \ln k_j$ , for most important reactions. Same conditions as in Figure 4.

first-order reactions with rate constant  $k_w = \gamma \bar{v} / D$ ,  $\gamma$  being the recombination coefficient,  $\bar{v}$  the thermal average velocity of the species considered, and  $D$  the reactor tube diameter.

Calculations were performed with wall reactions for all atoms and radicals in the reaction scheme of Table II at various values of the coefficient  $\gamma$ . The results of these calculations can be summarized as follows: for H, O, and OH, which rapidly react with various molecular species like  $O_3$  and  $CH_4$ , the occurrence of wall reactions would produce less than 1% changes in the mole fractions of the stable products even with  $\gamma = 10^{-2}$ , which appears rather high. It is thus concluded that wall reactions of these species are unimportant. The same holds for CHO and  $CH_2OH$ , which rapidly react with molecular oxygen. For  $CH_3$  and  $CH_3O$ , a value of  $\gamma = 10^{-3}$  would be required to make wall reactions insignificant. With  $\gamma = 10^{-2}$ , still low decreases with up to a few percent would result for some product mole fractions. The largest influence from wall recombinations would be expected for the less-reactive peroxy radicals  $HO_2$  and  $CH_3O_2$ . With  $\gamma = 10^{-3}$ , decreases up to 5% are calculated for some product mole fractions. These changes are minor and would not alter the main conclusions of this study.

Unfortunately,  $\gamma$  values are only known to some extent for atoms, so that it is difficult to come to a definite conclusion for the peroxy radicals. However, direct arguments for a low influence of wall reactions of these species are provided by the experimental observations. The immediate stable products of both radicals,  $H_2O_2$  and  $CH_3OOH$ , are clearly observed experimentally and reasonably well modeled by the homogeneous reaction mechanism. It is therefore concluded that wall reactions can only be of minor importance in this study.

**Sensitivity Analysis.** A kinetic sensitivity analysis was performed to find the most influential reactions in the scheme of Table II. The frequency factor of each rate constant in the table was divided by 5 and the new mole fractions resulting from the calculation were used to compute integral sensitivity coefficients  $S_{ij} = \Delta \ln x_i / \Delta \ln k_j$ . The results of such calculations for the most influential reactions at a maximal temperature of 833 K are shown in Figure 5. It is seen that reactions about which there is quite different knowledge are the most important. Apart from the fourth reaction, the reactions listed in Figure 5 can be grouped into three categories: (1) reactions involving ozone, (2) reactions of O and OH with  $CH_4$  and  $CH_2O$ , and (3) reactions of  $CH_3$ ,  $CH_3O$ , and  $CH_3O_2$ , many of the radical-radical type.

One of the most important reactions is the reaction of  $O_3$  with  $CH_3$ . Enhancing the rate constant of this reaction decreases all product concentrations except that of  $CH_2O$ , for which the influence is small. The reaction of  $O_3$  with H atoms, immediately following the reaction with  $CH_3$ , has a similar, but less pronounced, effect. The reason for decreasing the product concentrations is that the two reactive species  $O_3$  and  $CH_3$  are replaced by stable compounds and only one H atom that furthermore mostly destroys one more  $O_3$  molecules in the consecutive reaction. Since  $CH_2O$  is a direct product of the reaction, there is a compensating effect for this compound. Another potentially important aspect exists for the  $CH_3 + O_3$  reaction. If some  $CH_3O$  were also produced by this reaction, it could become a major source of this radical

which could alter the importance of the other reactions producing methoxy. The reason for taking  $CH_2O + H$  as products has been given above.

Of similar importance as the  $CH_3 + O_3$  reaction are the reactions of OH and O with methane, the main fuel consumption reactions. Fortunately, the rate constants of these reactions are rather well established. The reactions of O and OH with formaldehyde, the main carbon-containing product of the reaction, are also seen to be quite important, despite its much lower concentration. The reason for this is the greater reactivity of  $CH_2O$  toward O and OH compared with  $CH_4$ . Among the other reactions a number of radical-radical reactions are present whose rate constants have not been determined directly and therefore have been adjusted in this work.

Apart from the rate constants, a further important parametric sensitivity exists to the initial ozone concentration. All product mole fractions shown positive sensitivity coefficients with values from 0.5 to 1.2, in accordance with the experimental observations. The error in determining the initial ozone concentration, estimated at about 3%, will therefore result in uncertainties of the computed mole fractions of a few percent.

The results of the sensitivity analysis served as a basis for improving the agreement between measurements and calculations. This was not an easy exercise, however. It is apparent from Figure 5 that alterations of many rate constants influence more than one product concentration simultaneously. Especially for  $CH_3OH$  a balance had to be found between several reactions. Since many of the rate constants of the reactions listed in Figure 5 have been measured directly, their rate constants were only varied within the error estimates from these determinations. Only the rate constants of the radical-radical reactions 22, 31, and 33 were treated as essentially free parameters. Since the computed mole fraction of  $CO_2$  depends very sensitively on reaction 35, the only reaction producing  $CO_2$ ,  $k_{35}$  can be adjusted without appreciably influencing other products. Because no calibrations were possible, no attempts could be made to improve the fit for the peroxides apart from lowering the preexponential factor of reaction 24, which gives some improvement in the maximum of the  $CH_3OOH$  mole fraction with temperature.

The modifications finally arrived at are indicated in Table II. The rate constants obtained for reactions 22, 31, and 33 appear to be of reasonable magnitude. However, since there are still uncertainties in the mechanism, these values are tentative.

**Main Reaction Pathways.** The rather large mechanism of Table II per se cannot give easy insight into the main reaction pathways. The sensitivity analysis presented before has already given some clues as to the most important reactions. The results of the calculations, however, can be used to quantify the pathways by which the products are formed on a cumulative basis. A visualization of the importance of the reactions by which the carbon-containing compounds are formed is shown in Figure 6 for the same conditions as in Figure 4. It is seen that only about 30% of the ozone undergoes thermal decomposition to yield the O atoms that initiate the reaction. The remainder reacts almost exclusively with methyl radicals, produced by hydrogen abstraction by O and OH from methane, and with the hydrogen atoms produced by the  $CH_3 + O_3$  reaction. Of the other possible ozone-radical reactions, only the one with O atoms is of minor importance. The well-known reactions with OH and  $HO_2$  and further possible reactions with  $CH_3O$  and  $CH_3O_2$ <sup>37</sup> are too slow. The methyl radicals produced from methane are in a temperature-dependent equilibrium with methylperoxy radicals. Although this equilibrium favors the formation of peroxy radicals in the temperature range of the main conversion (cf. Figure 4), the net reaction via  $CH_3O_2$  is relatively small. The largest portion is reaction with  $CH_3$ , by which about 10% of  $CH_3$  and  $CH_3O_2$  react further. Self-reaction of two peroxy radicals, reaction with O atoms, and formation of hydroperoxide are only minor routes. After the reaction with ozone, the reaction of  $CH_3$  with  $HO_2$ , the radical with the second highest concentration after  $CH_3O_2$ , is most important. This reaction leads to chain propagation since one hydroxy radical is formed and  $HO_2$  is re-formed mainly through

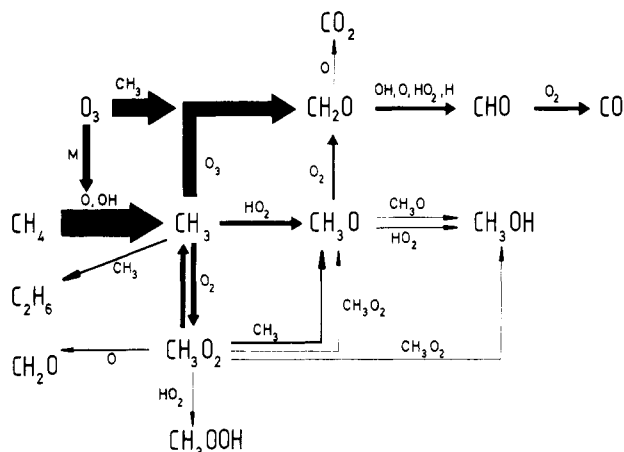


**Figure 6.** Main reaction pathways of carbon-containing compounds. The thickness of the arrows corresponds to contribution of the respective reaction. Same conditions as in Figure 4.

reaction 29. In a parallel reaction, a part of the methoxy radicals also reacts with itself and  $\text{HO}_2$  to form methanol.

From the temperature dependence of the formation of  $\text{CH}_2\text{O}$  and  $\text{CH}_3\text{OH}$  one might get the impression that these molecules do not undergo further reactions. But actually, a part of these compounds is attacked by the atoms and small radicals present. About 10% of the totally formed methanol reacts further in this way (not shown in Figure 5). For formaldehyde, this portion is

considerably higher: about one-third ultimately is transformed into carbon monoxide. The small amount of carbon dioxide formed can only be explained by the reaction between O and  $\text{CH}_2\text{O}$  forming  $\text{CO}_2$  directly, since the reactions of CO with OH and  $\text{HO}_2$  would represent just 3% of the amount actually observed. The observation of small amounts of  $\text{HCOOH}$  could represent a collisionally stabilized adduct of this reaction.

Two features of the ozone-initiated methane oxidation are brought out clearly by the analysis of the reaction mechanism. The first is the great importance of secondary reactions of ozone with reaction products, namely with methyl radicals and hydrogen atoms. The second is the striking dominance of radical-radical reactions. For the methyl radical, the reason is to be found in the low reactivity of this molecule with molecular oxygen apart from the addition reaction. The reaction  $\text{CH}_3 + \text{O}_2 \rightarrow \text{CH}_3\text{O} + \text{O}^{29}$  is too slow at these low temperatures. The situation is similar for the methylperoxy radical. A possible reaction of this species would be the propagation reaction  $\text{CH}_3\text{O}_2 + \text{CH}_4 \rightarrow \text{CH}_3\text{OOH} + \text{CH}_3$ , but this reaction is also too slow if one takes the same rate constant for it as for reaction 17. It thus appears that the low reactivity of methyl and methylperoxy radicals toward stable reaction partners strongly favors reactions with other radicals.

*Acknowledgment.* This work received financial support from the Deutsche Forschungsgemeinschaft. The calculations were performed at the Regionales Rechenzentrum für Niedersachsen. The author thanks B. Cochanski for help with the experiments.

Registry No.  $\text{CH}_4$ , 74-82-8.

## Excitation of Aromatic Hydrocarbons in Electron Beam Irradiated Rare Gas-Hydrocarbon Mixtures<sup>1</sup>

Lynette S. Denison,<sup>†</sup> Ronald Cooper,<sup>†</sup> and Myran C. Sauer, Jr.\*

Chemistry Division, Argonne National Laboratory, Argonne, Illinois 60439 (Received: August 9, 1985)

The technique of pulse radiolysis has been used to study the kinetics of formation and decay of emissions in aromatic hydrocarbon/rare gas systems. The mechanism for the formation of the  $S_1$  levels of anthracene, tetracene, and terphenyl in mixtures of the rare gases Ne, Ar, and Xe has been investigated. We have observed that, at low hydrocarbon pressures, the kinetics are adequately described by a sequential two-step process. The formation rate constant shows a linear dependence on hydrocarbon pressure and yields an overall rate constant for formation, in all systems studied, of approximately  $1 \times 10^{13} \text{ dm}^3 \text{ mol}^{-1} \text{ s}^{-1}$ . These rate constants are too large to be accounted for by atomic collisional energy-transfer processes and can only be interpreted in terms of subexcitation electrons being the immediate precursors of the  $S_1$  levels. The rates of decay were independent of pressure variations and reflected the radiative lifetimes of the  $S_1$  levels. A smaller effect of bulk rare gas pressure on the formation rate of the  $S_1$  levels is observed ( $\sim 10^9 \text{ dm}^3 \text{ mol}^{-1} \text{ s}^{-1}$ ) and is attributed to electron cooling by momentum-transfer processes.

### Introduction

In previous experiments on  $\text{N}_2$  in helium or neon, we have shown that subexcitation electrons can be responsible for the production of excited states in rare/trace additive mixtures.<sup>2</sup> The formation of the  $C^3\Pi_u$  state of  $\text{N}_2$  was observed to occur via a subexcitation electron mechanism at  $\text{N}_2$  pressures below 0.02 mmHg in mixtures of  $\text{N}_2$  in ultrapure helium and neon. In addition to the results presented for the  $\text{N}_2$ /rare gas systems, the results of preliminary studies on aromatic hydrocarbon/rare gas systems were also reported.

In the present study a more complete analysis of the processes responsible for the production of the  $S_1$  levels of anthracene, tetracene, and terphenyl in the mixtures of the rare gases Ne, Ar,

Kr, and Xe has been undertaken.

### Experimental Section

The system in this study was that developed for use with the Argonne National Laboratory Chemistry Division LINAC. This system has been described in detail in previous publications,<sup>3,4</sup> and only minor changes were made.

Kinetics of light emission were studied with a short (<40 ps) pulse of 20-MeV electrons with approximately 7 nC per pulse.

(1) Work performed under the auspices of the Office of Basic Energy Sciences, Division of Chemical Science, US-DOE, under contract No. W-31-109-ENG-38.

(2) Cooper, R.; Denison, L. S.; Sauer, M. C. Jr. *J. Phys. Chem.* **1982**, *86*, 5093.

(3) Sauer, M. C. Jr.; Mulac, W. A. *J. Chem. Phys.* **1972**, *56*, 4995.

(4) Cooper, R.; Greiser, F.; Sauer, M. C. Jr. *J. Phys. Chem.* **1976**, *80*, 2138.

<sup>†</sup> Department of Physical Chemistry, University of Melbourne, Parkville, Victoria, 3052, Australia.